

TABLE 1. ROSAT PSPC Pointings.

Pointing ¹	PI	α (J2000.0)	δ (J2000.0)	Exp Time ² s	Original Target	N_{PDCS} ³
wp201077	Fleming	00 27 39.7	+05 03 50.9	6373	PC 0025+0447	7
wp700165	Wendker	09 51 00.0	+47 39 49.4	1990	HS 47.5/22 FIELD	15
wp700173	Wendker	09 49 31.2	+47 15 00.0	1538	HS 47.5/22 FIELD	10
wp700174	Wendker	09 51 31.2	+47 15 00.0	2590	HS 47.5/22 FIELD	11
wp700175	Wendker	09 55 31.2	+47 15 00.0	2100	HS 47.5/22 FIELD	13
wp700176	Wendker	09 54 00.0	+47 30 00.0	2365	HS 47.5/22 FIELD	16
wp700177	Wendker	09 55 31.2	+46 45 00.0	1946	HS 47.5/22 FIELD	5
wp700178	Wendker	09 54 00.0	+47 00 00.0	2963	HS 47.5/22 FIELD	11
wp700179	Wendker	09 52 31.2	+47 45 00.0	6193	HS 47.5/22 FIELD	5
wp700450	Wendker	09 55 31.2	+47 45 00.0	3717	HS 47.5/22 FIELD	14
wp700452	Wendker	09 52 31.2	+47 45 00.0	2951	HS 47.5/22 FIELD	16
wp700453	Wendker	09 49 31.2	+47 45 00.0	4655	HS 47.5/22 FIELD	12
wp700455	Wendker	09 54 00.0	+48 00 00.0	3523	HS 47.5/22 FIELD	12
rp800238	Dressler	13 24 46.8	+30 35 02.9	24009	Distant Cluster	10

Notes to Table 1.

1. The ROSAT/PSPC pointing identification number. 2. The exposure time as given in the PSPC file header. 3. The number of PDCS cluster candidates within the central 40' of the field of view of the ROSAT PSPC.

TABLE 2. PDCS Cluster Candidates: X-ray Data.

PDCS ¹ #	α (J2000.0)	δ (J2000.0)	z ²	Aperture ³ (arcmin)	Exp. ⁴ (s)	N. Obs. ⁵	Count-Rate ⁶ (10^{-3} cts s $^{-1}$)	Aperture ⁷ Fraction	Status ⁸
01*	00 29 03.0	+05 01 24	0.6	2.1	4265	1	5.75	0.99	4.49
02	00 29 28.4	+05 04 03	0.4	2.6	4986	1	3.59	0.96	ul
03	00 28 36.6	+05 07 44	0.6	1.9	5579	1	2.51	0.99	ul
04	00 29 11.1	+05 08 55	0.5	2.2	4520	1	4.38	0.98	ul
05	00 27 38.6	+05 09 46	0.2	3.1	6305	1	3.57	0.99	ul
06	00 29 52.2	+05 12 36	0.4	3.3	4310	1	4.59	0.99	ul
08	00 28 31.4	+05 18 01	0.6	2.8	3632	1	2.27	0.30	ul
29	09 53 12.1	+47 08 58	0.4	2.4	17501	11	1.94	0.99	ul
30	09 54 46.3	+47 10 48	0.3	3.1	14472	9	2.79	0.99	ul
31	09 53 39.5	+47 12 58	1.1	1.9	17663	10	1.57	0.99	ul
32	09 52 29.0	+47 17 49	0.3	2.5	18784	11	1.82	0.83	ul
33*	09 52 13.1	+47 16 48	0.5	2.0	17481	10	3.19	0.84	5.07
34	09 55 09.1	+47 29 55	0.3	2.6	12190	7	2.83	0.99	ul
35	09 52 31.2	+47 36 27	0.6	1.8	17609	10	1.51	1.00	ul
36*	09 53 53.7	+47 40 15	0.3	2.4	14506	8	5.23	0.99	5.51
37	09 51 41.5	+47 41 30	0.6	1.9	14728	10	1.82	0.98	ul
38	09 51 09.9	+47 43 54	0.3	2.6	14639	9	1.98	0.99	ul
39	09 51 25.2	+47 49 50	0.6	2.1	11240	6	2.06	0.95	ul
40	09 53 25.6	+47 58 55	0.2	3.4	10077	9	3.30	0.58	ul
41	09 54 16.9	+47 58 41	0.7	2.5	9647	6	2.75	0.90	ul
42	09 53 54.2	+48 00 04	0.9	2.4	9399	6	2.46	0.88	ul
43	09 52 15.1	+47 57 44	0.2	3.4	11681	6	3.33	0.93	ul
44	09 52 18.6	+48 02 32	1.1	2.5	9988	6	2.21	0.97	ul
45	09 54 38.8	+47 15 59	0.4	2.4	15357	10	2.39	0.99	ul
57	13 23 47.3	+30 03 31	0.5	3.2	16063	1	1.44	0.25	ul
59	13 24 48.8	+30 11 36	0.751	2.1	16792	1	1.95	0.97	ul
60	13 23 39.0	+30 12 12	0.3	2.9	14779	1	2.43	1.00	ul
61*	13 27 07.4	+30 18 01	0.3	3.6	13787	1	4.09	0.47	4.40
62*	13 23 39.0	+30 22 26	0.4	2.3	14847	1	12.15	0.98	9.91
63*	13 24 20.6	+30 12 52	0.697	2.2	16011	1	2.17	0.37	4.71
64	13 26 22.3	+30 15 20	1.0	2.4	19302	1	1.74	1.00	ul

Notes to Table 2.

1. Identification number from the Palomar Distant Cluster Survey, asterisk denotes X-ray detection. 2. Estimated redshift derived from the V_4 band data (N.B. spectroscopic redshift quoted for 59 & 63). 3. The aperture radius in arcminutes. 4. The average exposure time over the aperture. 5. The number of PSPC observations combined to derive the count rate. 6. The count rate in the 0.4 – 2.0 keV passband. 7. The fraction of the total area in the aperture used for the flux determination. 8. Upper limits denoted by ul, signal to noise values quoted for detections.

TABLE 3. PDCS Cluster Candidates: Results.

PDCS ¹ #	Measured Flux	Fraction of Total Flux	Total Flux ²	z ³	L_x ⁴	Λ_{cl} ⁵	Status ⁶
01*	7.429	0.70	10.612	0.6	20.4	70.6	4.49
02	4.360	0.69	6.230	0.4	5.4	44.4	ul
03	3.250	0.70	4.643	0.6	8.9	88.5	ul
04	5.666	0.70	8.094	0.5	10.5	87.1	ul
05	4.600	0.70	6.571	0.2	1.2	31.8	ul
06	5.937	0.70	8.481	0.4	6.8	43.5	ul
08	2.949	0.58	5.085	0.6	9.8	75.3	ul
29	2.036	0.70	2.909	0.4	2.3	32.5	ul
30	2.927	0.70	4.181	0.3	1.8	46.5	ul
31	1.618	0.70	2.312	1.1	9.9	120.0	ul
32	1.915	0.67	2.859	0.3	1.3	32.2	ul
33*	3.346	0.67	4.995	0.5	6.5	41.3	5.07
34	2.964	0.70	4.234	0.3	1.9	62.0	ul
35	1.579	0.70	2.255	0.6	4.3	67.5	ul
36*	5.483	0.70	7.833	0.3	3.4	54.7	5.51
37	1.905	0.70	2.721	0.6	5.2	53.5	ul
38	2.085	0.70	2.979	0.3	1.3	47.7	ul
39	2.156	0.69	3.125	0.6	6.0	62.3	ul
40	3.467	0.59	5.877	0.2	1.1	28.3	ul
41	2.855	0.68	4.199	0.7	11.3	43.5	ul
42	2.540	0.67	3.792	0.9	17.7	61.0	ul
43	3.506	0.69	5.082	0.2	1.0	29.5	ul
44	2.276	0.70	3.251	1.1	23.6	173.1	ul
45	2.502	0.70	3.574	0.4	2.9	36.6	ul
57	1.533	0.35	4.381	0.5	5.7	73.7	ul
59	2.068	0.69	2.997	0.751	9.4	115.3	ul
60	2.596	0.70	3.709	0.3	1.6	34.1	ul
61*	4.378	0.48	9.116	0.3	4.0	33.2	4.40
62*	12.961	0.69	18.785	0.4	15.1	96.2	9.91
63*	2.304	0.44	5.236	0.697	14.0	103.7	4.71
64	1.835	0.70	2.621	1.0	15.4	81.6	ul

Notes to Table 3.

1. Identification number from the Palomar Distant Cluster Survey, asterisk denotes X-ray detection. 2. All fluxes are given in units of 10^{-14} ergs cm^{-2} s^{-1} in the 0.4 – 2.0 keV passband. 3. Estimated redshift derived from the V_4 band data (N.B. spectroscopic z quoted for 59 & 63). 4. X-ray luminosity in the 0.4 – 2.0 keV passband in units of 10^{43} ergs s^{-1} . 5. The PDCS matched filter richness. 6. Upper limits denoted by ul, signal to noise values quoted for detections.

X-ray Observations of Distant Optically Selected Clusters

B. P. Holden

Department of Astronomy and Astrophysics, University of Chicago, 5640 South Ellis Ave.
Chicago, Illinois 60637
holden@oddjob.uchicago.edu

A. K. Romer

Department of Physics, Carnegie Mellon University, 5000 Forbes Ave. Pittsburgh,
Pennsylvania 15213-3890
romer@astro.phys.cmu.edu

R. C. Nichol

Department of Physics, Carnegie Mellon University, 5000 Forbes Ave. Pittsburgh,
Pennsylvania 15213-3890
nichol@astro.phys.cmu.edu

M. P. Ulmer

Dearborn Observatory, Northwestern University, 2131 Sheridan Road, Evanston, Illinois
60208-2900
m-ulmer2@nwu.edu

ABSTRACT

We have measured fluxes or flux limits for 31 of the 79 cluster candidates in the Palomar Distant Cluster Survey (PDCS) using archival ROSAT/PSPC pointed observations. Our X-ray survey reaches a flux limit of $\simeq 3 \times 10^{-14}$ erg $\text{s}^{-1} \text{cm}^{-2}$ (0.4 - 2.0 keV), which corresponds to luminosities of $L_x \simeq 5 \times 10^{43}$ erg s^{-1} ($H_0 = 50 \text{ km s}^{-1} \text{Mpc}^{-1}$, $q_0 = \frac{1}{2}$), if we assume the PDCS estimated redshifts. Of the 31 cluster candidates, we detect six at a signal-to-noise greater than three. We estimate that $2.9^{+3.3}_{-1.4}$ (90% confidence limits) of these six detections are a result of X-ray emission from objects unrelated to the PDCS cluster candidates. The net surface density of X-ray emitting cluster candidates in our survey, $1.71^{+0.91}_{-2.19}$ clusters deg^{-2} , agrees with that of other, X-ray selected, surveys. It is possible, given the large error on our contamination rate, that we have not detected X-ray emission from any of our observed PDCS cluster candidates. We find no statistically significant difference between the X-ray luminosities of PDCS cluster candidates and those of Abell clusters of similar optical richness. This suggests that the PDCS contains objects at high redshift

similar to the low redshift clusters in the Abell catalogs. We show that the PDCS cluster candidates are not bright X-ray sources, the average luminosity of the six detected candidates is only $\bar{L}_x = 0.9 \times 10^{44}$ erg s⁻¹ (0.4-2.0 keV). This finding is in agreement with previous X-ray studies of high redshift, optically selected, rich clusters of galaxies.

1. Introduction

One of the focal points of modern observational cosmology is the study of how structure evolves. Clusters of galaxies provide an excellent probe of such evolution because they represent the largest gravitationally bound objects and can be identified over a large range of redshifts. X-ray surveys for clusters of galaxies have produced catalogs of physically massive objects, but most high redshift X-ray surveys are limited to small (~ 30) samples (Henry *et al.* 1992; Castander *et al.* 1995; Collins *et al.* 1997). By contrast, the availability of large format CCDs and sophisticated cluster finding algorithms means that it is now possible to produce optically selected catalogs, such as the Palomar Distant Cluster Survey (PDCS, Postman *et al.* 1996), which contain ~ 100 distant clusters with a large range of richnesses. In this paper we seek to compare the distant clusters found in automated optical surveys with those found with more traditional methods by studying the X-ray properties of the PDCS and by comparing the PDCS to lower redshift cluster samples.

Previous studies (Henry *et al.* 1982; Bower *et al.* 1994; Castander *et al.* 1994; Nichol *et al.* 1994; Sokoloski *et al.* 1996) have demonstrated that optically rich clusters at high redshift are often X-ray faint. Many of the clusters examined have velocity dispersions consistent with massive, bound, systems (Bower *et al.* 1997). The low luminosity of these systems has been cited as evidence for X-ray evolution in the cluster population (Bower *et al.* 1994). However, this interpretation may be premature, since the high redshift optical samples studied to date are extremely small and heterogeneously selected.

With our survey we are able to improve on previous X-ray studies of high redshift, optically selected, clusters. Our sample has the combined advantages of size (31 clusters in all), an objective cluster catalog (the PDCS) and random selection for the X-ray observations. We are also able to take advantage of two recent, low redshift ($z < 0.2$) X-ray surveys (Briel & Henry 1993; Burg *et al.* 1994) of Abell clusters (Abell 1958; Abell *et al.* 1989) which are both statistically complete and contain a large (~ 200) number of objects. Our sample should provide a fair representation of the X-ray properties of the PDCS as a whole and allow us to make direct comparisons with the Briel & Henry (1993) and Burg *et al.* (1994) surveys. Our survey will help us understand what sorts of galaxy overdensities

were selected as clusters by the PDCS and enable us to test for evolution in the cluster population.

In Sec. 2, we review the properties of the Palomar Distant Cluster Survey. Section 3 describes our analysis of the fourteen archival ROSAT/PSPC pointings that contain our X-ray data. We describe possible sources of contamination and compare with other published work in Sec. 4. We discuss our results in Sec. 5, and make conclusions in Sec. 6. Throughout this paper we assume $H_0 = 50 \text{ km s}^{-1} \text{ Mpc}^{-1}$ and $q_0 = \frac{1}{2}$.

2. The Palomar Distant Cluster Survey

The PDCS (Postman *et al.* 1996) was carried out using the 4-Shooter CCD Camera on the Hale 5m telescope in both the I_4 and V_4 bands (Gunn *et al.* 1987). The survey was compiled from scans in five different regions of the sky and covers a total of 5.1 deg^2 . The five fields were selected to have high Galactic latitude, low reddening and to avoid known, low redshift ($z < 0.1$), clusters. Throughout this paper we will refer to the fields by their respective hour of right ascension, *i.e.* $\alpha = 00^{\text{h}}, 02^{\text{h}}, 09^{\text{h}}, 13^{\text{h}}, \& 16^{\text{h}}$. The feature that sets the PDCS apart from previous searches for high redshift clusters (*e.g.* Gunn *et al.* 1986; Couch *et al.* 1991) is that it uses an automated matched filter technique to select cluster candidates from the galaxy catalog. This objective technique contrasts with the eye-ball methods used in the past and allows the authors to generate an accurate selection function based on simulations.

The PDCS catalog contains 79 entries and for each entry Postman *et al.* (1996) present several parameters. These include estimates of radius, redshift and richness. We make use of the PDCS estimated redshifts in Sec. 3 to calculate luminosities and to help define metric apertures within which source fluxes are measured. The estimated redshifts carry a large error, $\delta_z = 0.2$, and we discuss in Sec. 5 what impact these errors have on our conclusions. Also in Sec. 5, we make use of the PDCS matched filter richness estimate, Λ_{cl} , to examine the relationship between optical and X-ray cluster properties. We note that, for clusters with redshifts less than $z = 0.7$, the matched filter richness can be equated with the Abell richness (see Sec. 5 and Figure 21 of Postman *et al.* 1996).

Postman *et al.* (1996) have carried out extensive simulations to derive an estimate of the completeness and contamination of their catalog. They generated artificial galaxy maps designed to reproduce, as closely as possible, the background galaxy distribution in the five PDCS fields. The rate of false positive detections in these maps should represent the rate of contamination in the PDCS catalog. They plot, in Figure 18 of their paper, the false

positive rate as a function of both measured size and detection significance. Postman *et al.* (1996) estimate that the contamination level in the PDCS sample is at the 12%–31% level. They used a different set of simulations to investigate the completeness of their survey. They simulated $\gtrsim 10000$ clusters over a wide range in redshift, richness and projected radial profiles and conclude that, for clusters with Abell richnesses ≥ 1 , their catalog is complete over the range $0.2 \leq z \leq 0.6$. Their simulations included clusters that did not match their matched filter in radial profile, but all models were spherically symmetric.

In summary, the simulations carried out by Postman *et al.* (1996) have shown that the PDCS provides a sensitive way to identify optical cluster candidates. However, the simulations also highlight the need for optical spectroscopy and X-ray imaging to confirm the identity of the objects in the PDCS. We note that, since up to 31% of the objects in the PDCS catalog might not be real clusters, we will refer to the entries in this catalog as ‘PDCS cluster candidates’ throughout this paper.

3. The X-ray Data Analysis

We have searched the High Energy Astrophysics Science Archive Research Center (HEASARC) database for those ROSAT/PSPC pointings which have PDCS cluster candidates in their field of view. Fourteen such pointings were found and these are summarized in Table 1. We note that, at the time of writing, no ROSAT PSPC pointing data were available for the PDCS fields at 02^h or 16^h.

We reduced all fourteen pointings using the Extended X-ray Analysis Software (EXAS) of Snowden *et al.* (1994). EXAS corrects for the energy dependence of the vignetting function and the particle backgrounds. EXAS also removes time intervals where the total count rate was too high ($> 5.7 \text{ cts s}^{-1}$) or where an event was contaminated by a previous pulse. The software produces exposure maps, count maps and particle background maps in seven different energy bands (R1 through R7). For our analysis, we combined the maps in bands R3 through R7 to produce a single count-rate map and error map in the energy range 0.4 - 2.0 keV for each pointing. We excluded the lowest bands, R1 and R2, which cover the energy range 0.1 - 0.4 keV, to minimize the effects of absorption by Galactic hydrogen.

For a PDCS cluster candidate to be included in our sample, we required that its optical centroid be less than 40' from the PSPC pointing center. Moreover, the PSPC exposure time at the optical centroid had to exceed 3000 seconds. Thirty-one PDCS cluster candidates met these requirements. For each of candidates, we derived an aperture for the

flux measurement using a cluster model based on a modified isothermal sphere:

$$I = \frac{I_o}{[1 + (r/r_c)^2]^{3\beta-1/2}} \quad , \quad (1)$$

where I is the surface brightness at radius r . We used values for the slope ($\beta = \frac{2}{3}$) and core radius ($r_c = 250$ kpc) which are typical for rich clusters (Jones & Forman 1992). We converted the above model from physical units to angular units using the estimated redshifts from the PDCS unless a spectroscopic redshift was available. We then convolved the model with an appropriate PSPC point spread function (PSF), using the PSF model derived empirically by Nichol *et al.* 1994. We increased the radius of the aperture until the integrated flux within the aperture included 70% of the total flux of the PSF convolved model. This radius depends on the size of the PSF, but is approximately $3.5 \times r_c$. The aperture radii are listed in column five of Table 2 and range from $1.8'$ to $3.6'$.

Before measuring fluxes, we masked out certain aperture pixels. We masked those pixels that were common to more than one cluster aperture and those pixels that had less than 3000 seconds of exposure. (The latter tend to fall in the shadow of the PSPC window support structure.) We also ran a source detection algorithm on the 14 pointings. This allowed us to mask any pixels that contained flux from sources with centroids more than $2'$ (four times the uncertainty in the PDCS positions) from the PDCS cluster candidates. (The detection software provided outlines of the sources as well as centroid information.) We note that in two cases, PDCS 36 & 62, a source was detected within $2'$ of the PDCS candidate and that the pixels associated with these two sources were not masked. The source detection algorithm we used was that of the Serendipitous High-redshift Archival Cluster (SHARC) Survey and is more completely described in Freeman *et al.* 1995 and Nichol *et al.* 1997.

In total, 16 of the 31 apertures were masked in some way. In four cases, more than $\simeq 50\%$ of the aperture was masked. The fraction of the aperture left available for flux derivation is listed in column nine of Table 2. For those clusters covered by multiple pointings (all those at $\alpha = 09^h$), this column lists the maximum aperture fraction available from among the individual observations. The count-rate for each of the 31 PDCS cluster candidates was measured by summing the flux in the unmasked aperture pixels. The corresponding background count-rates were measured in annuli covering 1.5 times the area of, and surrounding, the unmasked apertures. The background apertures were masked, where appropriate, following the rules described above.

The PDCS cluster candidates in the collection of pointings at $\alpha = 09^h$ required special treatment. These 17 objects were observed multiple times (see Table 2 column seven) but always at different positions on the PSPC. To maximize the effective amount of exposure

time for these clusters, we combined the (background subtracted) count-rate measurements from each observation via a weighted average to produce a mean, background subtracted, count-rate for each source. The weights were the product of the average exposure time and the fraction of the total aperture used.

With all background subtracted count-rates in hand, we then determined which of the 31 observations could be classified as detections. For this we used the (0.4 - 2.0 keV) error map from the EXAS package to compute the error, in counts per second, in each (masked) aperture. (The errors for the $\alpha = 09^{\text{h}}$ objects were derived by combining the errors on the individual observations in a weighted fashion.) We classified any observation as a detection if the ratio of the background subtracted count-rate to the error was greater than three ¹ Six observations met this criterion and they are marked with an asterisk in Table 2, column one, and illustrated in Figure 1. Also in Table 2, we list the background subtracted count-rate (column eight) and the signal-to-noise ratio of the detection (column ten). For the 25 PDCS cluster candidates that were not detected, we list an upper limit to their background subtracted count-rate given by three times the measured error.

We converted our measured count-rates (or 3σ upper limits) to energy fluxes by integrating a redshifted 6.0 keV thermal *bremsstrahlung* spectrum over our energy passband of 0.4 - 2.0 keV. All fluxes were then corrected for absorption using the observed amount of Galactic neutral hydrogen in the AT&T Bell Laboratories 21 cm survey (Stark *et al.* 1992) and the cross-section values from Morrison & McCammon (1983). Once we had the energy flux inside the masked aperture (column two of Table 3), we needed to convert to a total flux for each cluster candidate. For cluster apertures where no part of the aperture was masked, the energy flux was simply divided by 0.7 (see previous discussion) to give a total flux (column four of Table 3). For the apertures that were masked, we computed the fraction of the flux from our model that would fall within the masked aperture and then used this fraction to convert between measured and total flux. The aperture corrections used to convert between measured and total flux are listed in Table 3, column two. The luminosities are presented in units of 10^{43} erg s⁻¹ in Table 3, column six.

4. Sources of Error

Clusters of galaxies represent only a small fraction of the astronomical objects that emit X-rays. We have therefore investigated how accidental coincidences between non-cluster sources and PDCS cluster candidates effect the results in Table 3. In Sec. 4.1, we calculate

¹We note here that this paper uses a different definition of detection than the SHARC Survey.

the number of non-cluster objects expected to fall in our apertures using established logN-logS relations. In Sec. 4.2, we highlight the detections which are most likely to be of contaminating sources. In Sec. 4.3, we compare our methodology to that of Castander *et al.* (1994). Finally, in Sec. 4.4, we discuss the surface density and redshift distribution of X-ray emitting clusters in our sample as a measure of our completeness.

4.1. Expected contamination

Using the logN-logS relation derived from the UK Deep and Medium Surveys with ROSAT (Branduardi-Raymont *et al.* 1994), we were able to estimate the number of non-cluster source detections in our survey. For each of the 31 PDCS cluster candidates, we used the 3σ flux limit and the integrated the logN-logS to compute the number of objects expected per unit angular area. To derive the area for each source, we used the aperture size (Column 9 of Table 2 or $2'$, if this was smaller. (Sources lying more than $2'$ from the PDCS centroid are excluded from our apertures, see Sec. 3.) We then multiplied the area of aperture by the fraction of the area used in the actual flux determination (Column 9 of Table 2) to determine angular area the aperture subtended. The results from the 31 calculations were summed to give a contamination level of $2.9_{-1.4}^{+3.3}$ sources (90% confidence limits). This level of contamination is quite high and it is possible that all of the detections flagged in Table 3 correspond to non-cluster sources. We repeated the measurements of Section 3 but with a cutoff radius of $1.5'$ or three times the estimated error in the PDCS positions, instead of the above $2'$. Our calculated error decreases to $2.1_{-1.0}^{+2.4}$ sources (90% confidence limits). However, PDCS 01 is no longer considered a detection in this sample. This leaves the net number of detections approximately the same. Therefore, our estimate of the net number of X-ray detections associated with PDCS cluster candidates appears to be insensitive to the details of the X-ray analysis.

4.2. Possible Identification of Non-cluster X-ray Sources

We searched the NASA/IPAC Extragalactic Database (NED, Helou *et al.* 1991) for possible sources of non-cluster X-ray emission near to our six detections (PDCS 01, 33, 36, 61, 62, & 63). For PDCS 01, nothing was found within $5'$ of the PDCS position. A radio source is located $2'$ away from PDCS 33, but this object is not coincident with the detected X-ray emission. For PDCS 36, the optical and X-ray centroid are coincident and there are no nearby likely sources of X-ray emission listed in NED. There are three FIRST (Becker *et al.* 1995) radio sources within $5'$ of PDCS 61 and all of these lie in the vicinity of the strong

X-ray emission to the north west of the PDCS centroid. An elliptical galaxy lies $3.3'$ from PDCS 62, but this object is further from the X-ray centroid than the cluster candidate (the latter have a separation of only $0.9'$). For PDCS 63, no nearby optical or radio source was found in NED. Based on this search, and on the comparison of optical and X-ray positions, we find it probable that the cluster candidate is the source of the detected X-ray emission in the case of PDCS 01, 36, 62, & 63. The other detections, around PDCS 33 & 61, might be due to contaminating sources. However, these results are subjective and cannot be confirmed without optical spectroscopy. Therefore, for the remainder of this paper, we will assume the contamination levels derived statistically in Sec. 4.1.

4.3. Comparison with Castander *et al.* 1994

In this section, we compare the results of our X-ray analysis to those from an X-ray survey by Castander *et al.* (1994) of high redshift GHO clusters (Gunn *et al.* 1986). We have two clusters in common with this survey, PDCS 59 and 63. For PDCS 63, or Cl1322+3029, Castander *et al.* (1994) reported a 3.0σ detection and a luminosity of $7.3 \pm 2.2 \times 10^{43}$ (0.1 - 2.4 keV) erg s⁻¹. We measure a 4.7σ detection and a luminosity of $L_x = 14.0 \pm 3.0 \times 10^{43}$ (0.4 - 2.0 keV) erg s⁻¹. We attribute this difference to the bright X-ray source which lies $2.5'$ from PDCS 63, see Figure 1. The manner in which this source is masked from the detection and background apertures strongly effects the flux measured for PDCS 63. The difference between our luminosity measurement for PDCS 63 and that of Castander *et al.* (1994) is not significant since the statistical error we quote most probably underestimates the uncertainty in the measurements.

Our results for PDCS 59, or Cl1322+3027, also differ. Castander *et al.* (1994) report a 3.1σ detection while we have a 2.0σ result. We have found that this discrepancy is largely a result of the differences between the software package (EXAS) we used compared to that (SASS) used by Castander *et al.* (1994). Most of the difference between our result and the result of Castander *et al.* (1994) stems from the rejection of time intervals by EXAS where the threshold count rate of 5.7 cts s⁻¹ was exceeded (see Sec. 3 for details). Using the SASS produced maps instead of the EXAS software, we measure a 3.0σ flux for PDCS 59.

For PDCS 59, Castander *et al.* (1994) measure a luminosity which is 1σ below the 3σ upper limit quoted in Table 3; $L_x = 6.7 \pm 2.1 \times 10^{43}$ (0.1 - 2.4 keV) erg s⁻¹ compared to $L_x = 9.4 \times 10^{43}$ (0.4 - 2.0 keV) erg s⁻¹. Our measured error is 1.5 times higher than that measured by Castander *et al.* (1994) and we believe this is a consequence of the EXAS removal of events falling in bad time intervals. Whether or not PDCS 59 meets the criteria for detection depends sensitively on how we calculate the background and how we

attempt to eliminate systematic errors. For the remainder of the paper we will make the conservative assumption that PDCS 59 was not detected.

As our results differ with Castander *et al.* (1994) for both PDCS 59 and 63, we decided to apply our X-ray analysis to 3 other clusters, Cl 1322+3115, Cl 1603+4313, and Cl 1603+4329. These clusters are not in the PDCS, but the relevant, EXAS reduced, PSPC pointings were available to us via the SHARC Survey. We conducted the same analysis discussed in Sec. 3 on these clusters, and in all three cases we find our error to be higher than that published in Castander *et al.* (1994). Despite this, we agree with Castander *et al.* (1994) as to the status of these clusters; we measure only upper limits for Cl 1322+3115 and Cl 1603+4329 and, for Cl 1603+4313, we register a 4.7σ detection. (Castander *et al.* 1994, quote a similar - 4.3σ - detection for this cluster.) In conclusion, we have found that our X-ray analysis does not differ significantly from that of Castander *et al.* (1994) and that we agree on the the detection or non-detection of 4 out of 5 objects in the Castander *et al.* (1994) sample. We do find a systematic difference in the measurement of the error for our sources. This causes a corresponding increase in the measured luminosity or luminosity upper limit. However, most of the apparent dissimilarities are at the $1 - 3\sigma$ level. These are attributable to the use of differing software packages and background measurement techniques.

4.4. Surface Density and Completeness

The angular overlap between the 14 PSPC pointings we used and the 5 PDCS survey fields was 1.85 deg^2 . The majority of this area, 1.38 deg^2 , was surveyed to a flux limit of $\simeq 3 \times 10^{-14} \text{ ergs s}^{-1} \text{ cm}^{-2}$ (0.4 - 2.0 keV). We have derived the surface density of X-ray clusters in this 1.38 deg^2 area and compared it to previous results. Of the six detections listed in Table 3, five lie in this study area. We have repeated the calculation described in Sec. 4.1 for this area and flux limit. We derive an expectation value of $2.64_{-1.26}^{+3.02}$ chance coincidences of non-cluster X-ray sources with PDCS cluster candidates. The net number ($2.36_{-3.02}^{+1.26}$) of X-ray emitting clusters over the 1.38 deg^2 area yields a surface density of $1.71_{-2.19}^{+0.91}$ clusters deg^{-2} to a limiting flux of $\simeq 3.0 \times 10^{-14} \text{ ergs s}^{-1} \text{ cm}^{-2}$ (0.4 - 2.0 keV). A number of surveys have been conducted to similar limiting fluxes over areas on the order of 15 deg^2 (Castander *et al.* 1995, Rosati *et al.* 1995, Scharf *et al.* 1997, Collins *et al.* 1997). Although not all of these groups have completely identified their sources, most report between 2 and 3 clusters deg^{-2} . The lowest reported surface density is $\sim 1 \text{ deg}^{-2}$ from Castander *et al.* (1995). Our result, of $1.71_{-2.19}^{+0.91}$ clusters deg^{-2} , is therefore in good agreement with other surveys, especially considering the large error on our contamination

rate (see Sec. 4.1). We conclude that it is unlikely that our survey has missed any X-ray emitting clusters, though we cannot rule out that possibility.

Using the photometrically estimated redshifts from the PDCS, we find the range of luminosities for the detected PDCS candidates to be $0.34 < L_x < 2.00 \times 10^{44}$ erg s⁻¹, with $\bar{L}_x = 0.9 \times 10^{44}$ ergs s⁻¹ (0.4 - 2.0 keV). These values are consistent with those derived from other X-ray cluster surveys constructed from PSPC pointings to similar flux limits. Assuming the PDCS photometric redshifts are not systematically biased, the redshift distribution of the six candidate X-ray clusters in our sample roughly agrees with that measured by Collins *et al.* (1997). The redshift range of these 6 objects is $0.3 < z < 0.69$, with $\bar{z} = 0.46$. We conclude that the objects in our survey are similar, in terms of surface density, luminosity range and redshift distribution, to those found in X-ray selected distant cluster samples.

5. Discussion

Our X-ray survey of 31 PDCS cluster candidates has resulted in 6 detections and 25 upper limits. We have combined both the detections and the upper limits to study the relation between X-ray luminosity and optical richness for PDCS clusters. We have compared this relation to that derived from lower redshift samples to understand what sort of galaxy overdensities were selected by the PDCS.

In Figure 2 we plot the richness, Λ_{cl} , measured from the PDCS (see Sec. 2.) versus the estimated X-ray luminosity, L_x , corresponding to the detections and upper limits. As the PDCS was conducted in two different passbands, each cluster candidate has two values for Λ_{cl} and both are shown in the figure. Using the techniques outlined in Isobe *et al.* (1986) as implemented in the STSDAS survival analysis package, we can test our data for a correlation. We measure a correlation between L_x and richness at the 96.6% confidence limit for the V_4 band and at the 93.2% confidence limit for I_4 band. This is in contrast to the strong correlation, at the $\geq 99.95\%$ confidence level, measured for Abell clusters (Abramopoulos & Ku 1983, Kowalski *et al.* 1984; Briel & Henry 1993). We note that the analysis of Kowalski *et al.* (1994), like that used here, combined both detections and upper limits. The lack of a statistically significant correlation ($> 99.95\%$) in our data could be a reflection of several systematic biases in our sample; contamination by non-cluster X-ray sources, the error in the PDCS distance estimates, or errors in our flux measurements.

We have also plotted on Figure 2 (solid line), the fitted L_x versus richness relation for Abell clusters taken from Briel & Henry (1993). We have adjusted this relation to

take account of the differing passbands of our work compared to that of the ROSAT All Sky Survey, but have assumed that the PDCS richness (Λ_{cl}) is equal to the Abell richness (N_{Abell} , see Sec. 2). The dashed lines on Figure 2 represent the median luminosities for Richness class 0, 1, & 2 Abell clusters taken from Burg *et al.* (1994), after appropriate conversion from the Einstein IPC detector passband (0.5 - 4.5 keV). Although care must be taken in interpreting Figure 2, since the majority of our data points are upper limits, it does seem to illustrate that our data have a similar X-ray luminosity distribution to that of low redshift clusters.

One of the largest sources of uncertainty in our luminosity versus richness analysis is the error in the estimated redshift, which can be as large as $\delta_z \sim 0.2$. Therefore, we now consider a redshift independent quantity that measures the correlation between optical and X-ray luminosities. We used the ratio of the optical luminosity to the X-ray luminosity (L_{opt}/L_x), where L_{opt} is defined as the optical richness, Λ_{cl} , multiplied by the absolute luminosity of an L_* galaxy in the V_4 band, as specified in Table 3 of Postman *et al.* (1996). The resulting ratio is not truly redshift independent, since the apertures used to construct the optical richness and X-ray luminosity values require a redshift estimate, but redshift dependence has been minimized. This method has been used previously by Stocke *et al.* (1991) to measure L_{opt}/L_x ratios for EMSS clusters, though we note that the ratio we use here is slightly different. Whereas we define optical luminosity using the bright end of the cluster member luminosity function, Stocke *et al.* (1991) relied only on the magnitude of the brightest cluster galaxy.

We plot, in Figure 3, the L_{opt}/L_x ratio as a function of estimated redshift for the 31 PDCS cluster candidates in our sample. We also plot the L_{opt}/L_x ratio for the Abell clusters in the Briel & Henry (1993) survey. For these clusters, L_{opt} is given by the Abell richness, N_{Abell} , multiplied by L_* . (Both Λ_{cl} and N_{Abell} correspond to the number of L_* galaxies in a 3.0 Mpc radius.) From Figure 3, it is apparent that the L_{opt}/L_x ratios of the detections in our survey are similar to those of Abell clusters in Briel & Henry (1993). We have performed a number of statistical tests (the Gehan, logrank, Peto-Peto, and the Peto-Prentice tests, see Sec. III of Schmitt 1985 for a discussion of statistical tests comparing two samples with censoring) using the STSDAS survival analysis package to compare the distributions of the ratio for the 2 samples. Although it might appear that the ratio of X-ray luminosity to optical luminosity is, on average, slightly lower in the PDCS sample, we found no statistically significant ($> 95\%$) difference between the PDCS sample and the sample of Briel & Henry (1993) in any of the four different tests we tried. We note that the apparent downturn in the L_{opt}/L_x ratio for the PDCS sample at $z \gtrsim 1.0$, coincides with the redshift at which the PDCS catalog becomes incomplete.

In summary, for the 31 PDCS cluster candidates in our sample, we do not measure a statistically significant correlation between L_x and richness. Comparisons with the Briel & Henry (1993) and Burg *et al.* (1994) surveys, illustrate that our clusters are not dissimilar - in terms of their luminosity range at a given richness - to Abell clusters at lower redshifts. Using a redshift independent test involving optical to X-ray luminosity ratios, we have found no significant difference between PDCS and Abell clusters. Both samples, PDCS and Abell, demonstrate a wide range in optical to X-ray luminosities at a given redshift or optical richness.

6. Conclusions

We have searched for X-ray emission around 31 distant, optically selected, rich clusters of galaxies taken from the PDCS sample of Postman *et al.* (1996). We have found six possible coincidences between PDCS clusters and X-ray sources detected in ROSAT/PSPC pointings. Our statistical analysis, and explicit searches for alternative optical or radio counterparts to the X-ray sources, are consistent with 3 of these 6 being detections of contaminating, non-cluster, sources.

Our survey demonstrates that PDCS cluster candidates are not strong ($L_x \gtrsim 5 \times 10^{43}$ erg s⁻¹) X-ray emitters. This observation is consistent with the results of previous studies of distant, optically selected, clusters (Bower *et al.* 1994; Castander *et al.* 1994; Nichol *et al.* 1994; Sokoloski *et al.* 1996) and highlights the possible existence of a population of optically rich clusters which are X-ray faint. The average luminosity of the six detections in our survey, $\bar{L}_x = 0.9 \times 10^{44}$ ergs s⁻¹, and the estimated surface density of X-ray emitting clusters in the PDCS fields, 1.71 deg⁻², are consistent with the results of previous surveys for distant, X-ray selected, clusters (Castander *et al.* 1995; Rosati *et al.* 1995; Scharf *et al.* 1997; Collins *et al.* 1997).

Taking both the upper limits and the detections, we find no statistically significant correlation between optical richness and X-ray luminosity in our sample, in contrast to the strong correlation ($\geq 99.95\%$ confidence level) measured previously for Abell clusters (Abramopoulos & Ku 1983; Kowalski *et al.* 1984; Briel & Henry 1993). This is not surprising given the large uncertainties in the redshifts of the PDCS. We find that our sample is in agreement with that of Briel & Henry (1993) when we compare optical to X-ray luminosity ratios, which is a redshift independent test. Our data are, therefore, consistent with the hypothesis that the PDCS and the Abell catalog sample the same section of cluster population, albeit at different redshifts. Furthermore, we find no evidence for evolution in the X-ray versus optical properties of rich clusters out to a redshift of $z = 0.6$.

The combination of the X-ray data presented here with the objective selection of the PDCS, makes this sample of 31 distant clusters ideal for further studies of cluster evolution. We are actively engaged in following up this sample with photometry and spectroscopy. These new data will allow us not only to determine which cluster candidates represent real physical systems, but also to estimate the volume density of X-ray emitting clusters and to probe the relationship between velocity dispersion and X-ray luminosity. These various studies will allow us to quantify the degree to which cluster properties are evolving with redshift.

7. Acknowledgments

We are extremely grateful to many people for stimulating discussions during this work. We thank the Lori Lubin, Constance Rockosi, Francisco Castander and Marc Postman for their time and helpful comments. We would like to especially thank Rich Kron for his careful readings of earlier manuscripts and suggested improvements in the analysis. Finally, we thank an anonymous referee for their careful reading of the paper and their constructive comments. BH was supported in part by the National Science Foundation under a cooperative agreement with the Center for Astrophysical Research in Antarctica (CARA), grant number NSF OPP 89-20223. CARA is a National Science Foundation Science and Technology Center. AR and MU acknowledge support from NASA ADP grant NAG5-2432. This research has made use of data obtained through the High Energy Astrophysics Science Archive Research Center Online Service, provided by the NASA-Goddard Space Flight Center. This research has made use of the NASA/IPAC Extragalactic Database (NED) which is operated by the Jet Propulsion Laboratory, Caltech, under contract with the National Aeronautics and Space Administration.

REFERENCES

- Abell, G. O., 1958, *ApJS*, 3, 211.
- Abell, G. O., Corwin, H. G. JR, Olowin, R. P., 1989, *ApJS*, 70, 1.
- Abramopoulos, F., & Ku, W. 1983, *ApJ*, 271, 446.
- Becker, R. H., White, R. L., & Helfand, D. J. 1995, *ApJ*, 450, 559.
- Bower, R. G., Böhringer, H., Briel, U. G., Ellis, R. S., Castander, F. J., & Carter, D. 1994, *MNRAS*, 268, 345.

- Bower, R. G., Castander, F. J., Couch, W., Ellis, R. S., & Böhringer, H. 1997, MNRAS, accepted.
- Branduardi-Raymont, G., Mason, K. O., Warwick, R. S., Carrera, F. J., Graffagnino, V. G., Mittaz, J. P. D., Puchnarewics, E. M., Smith, P. J., Barber, C. R., Pounds, K. A., Stewart, G. C., Hardy, I. M. M., Jones, L. R., Merrifield, M. R., Fabian, A. C., Mahon, R. G. M., Ward, M. J., George, I. M., Jones, M. H., Lawrence, A., & Rowan-Robinson, M. 1994, MNRAS, 270, 974.
- Briel, U. G., & Henry, J. P. 1993, A&A, 278, 379.
- Burg, R., Giacconi, R., Forman, W., & Jones, C. 1994, ApJ, 422, 37.
- Castander, F. J., Ellis, R. S., Frenk, C. S., Dressler, A., & Gunn, J. E. 1994, ApJ, 424, L79.
- Castander, F. J., Bower, R. G., Ellis, R. S., Aragon-Salamanca, A., Mason, K. O., Hasinger, H., McMahon, R.G., Carrera, F.J., Mittaz, J. P. D., Perez-Fournon, I., & Lehto, H. J. 1995, Nature, 377, 39.
- Collins, C. A., Burke, D. J., Romer, A. K., Sharples, R. M., & Nichol, R. C. 1997, ApJ, 479, L117.
- Couch, W. J., Ellis, R. S., MacLaren, I. & Malin, D. F. 1991, MNRAS, 249, 606.
- Freeman, P.E., Kashyap, V., Rosner, R., Nichol, R., Holden, B., & Lamb, D.Q. 1995, ADASS V, eds. G. Jacoby & J. Barnes, 101, 163.
- Gunn, J. E., Hoessel, J. G., & Oke, J. B. 1986, ApJ, 306, 30.
- Gunn, J. E., Emory, E. B., Harris, F. H., & Oke, J. B. 1987, PASP, 99, 518.
- Helou, G., Madore, B.F., Schmitz, M., Bica, M.D., Wu, X. & Bennett, D. 1991, in Databases and On-Line Data in Astronomy, ed. D. Egret & M. Albrecht (Dordrecht: Kluwer), p. 89.
- Henry, J. P., Soltan, A., Briel, U., & Gunn, J. E. 1982, ApJ, 262, 1.
- Henry, J. P., Gioia, L., Maccacaro, T., Morris, S. L., Stocke, J., & Wolter, A. 1992, ApJ, 386, 408.
- Isobe, T., Feigelson, E.D., & Nelson, P.I. 1986, ApJ, 306, 490.
- Jones, C., & Forman, W. 1992, in Clusters and Superclusters of Galaxies, ed. A. C. Fabian (Dordrecht: Kluwer), p. 49.

- Kowalski, M., Ulmer, M., Cruddace, R., & Wood, K. 1984, *ApJS*, 56, 403.
- Morrison, R., & McCammon, D. 1983, *ApJ*, 270, 119.
- Nichol, R. C., Ulmer, M. P., Kron, R. G., Wirth, G., & Koo, D. C. 1994, *ApJ*, 432, 464.
- Nichol, R. C., Holden, B. P., Romer, A. K., Ulmer, M. P., Burke, D. J., & Collins, C. A. 1997, *ApJ*, 481, 644.
- Postman, M. P., Lubin, L. M., Gunn, J. E., Oke, J. B., Hoessel, J. G., Schneider, D. P., & Christensen, J. A. 1996, *AJ*, 111, 615. (PDCS)
- Rosati, P., Della, Ceca, R., Burg, R., Norman, C., & Giacconi, R. 1995, *ApJ*, 445, L11.
- Scharf, C., A., Jones, L. R., Ebeling, H., Perlman, E., Malkan, M., Wegner, G. 1997, *ApJ*, 477, 79.
- Schmitt, J. H. M. M. 1985, *ApJ*, 293, 178.
- Sokoloski, J. L., Daly, R. A., Lilly, S. J. 1996, *ApJ*, 459, 142.
- Snowden, S. L., McCammon, D., Burrows, D. N., & Mendehall, J. A., 1994, *ApJ*, 424, 714
- Stark, A. A., Gammie, C. F., Wilson, R. W., Balley, J., Linke, R. A., Heiles, C., & Hurwity, M. 1992, *ApJS*, 79, 77.
- Stocke, J. T., Morris, S. L., Gioia, I. M., Maccacaro, T., Schild, R., Wolter, A., Fleming, T. A., & Henry, J. P. 1991, *ApJS*, 76, 813.

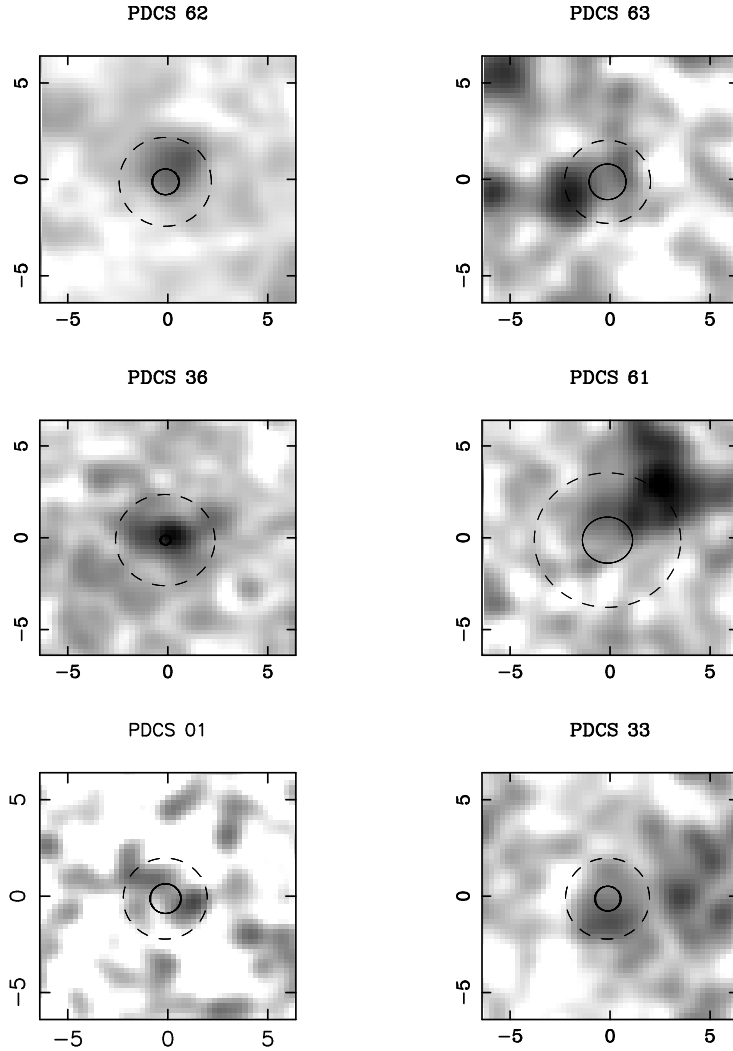


Fig. 1.— X-ray images of the six PDCS cluster candidates in our survey that are coincident with $> 3\sigma$ detections. Each image is $12.7'$ on a side and centered on the PDCS optical centroid. The darkest grey scale represents 1.7×10^{-14} ergs $\text{s}^{-1} \text{cm}^{-2} \text{arcmin}^{-2}$, while the lightest grey scale represents 2.7×10^{-15} ergs $\text{s}^{-1} \text{cm}^{-2} \text{arcmin}^{-2}$, with logarithmic scaling between these values. For PDCS 62, the darkest greyscale represents 1.07×10^{-13} ergs $\text{s}^{-1} \text{cm}^{-2} \text{arcmin}^{-2}$. The inner circle, represented by a solid line, is the half light radius of the corresponding off-axis point spread function. The outer circle, a dashed line, shows the unmasked aperture used to calculate the flux for the object. The tick marks represent 5 arcminutes of angle.

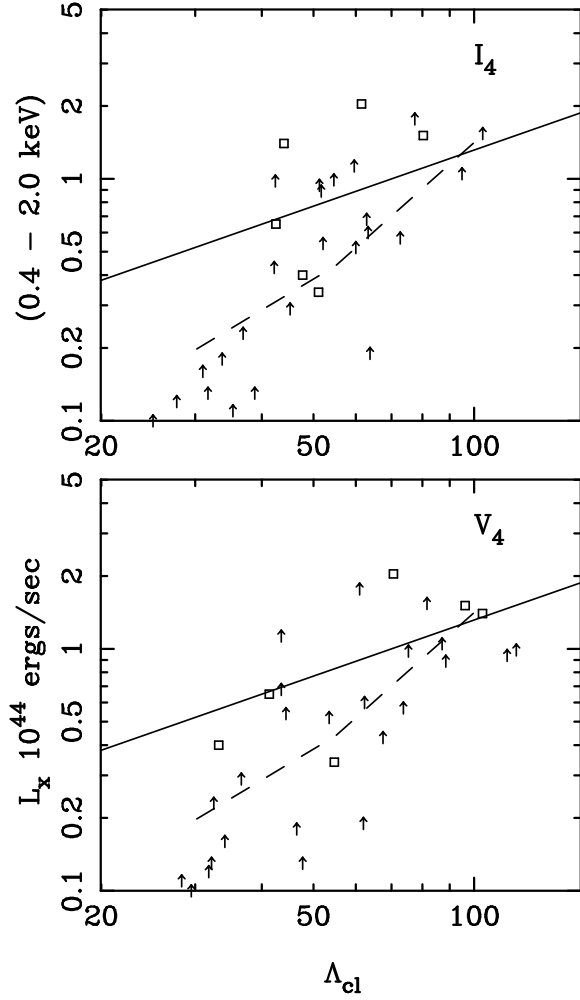


Fig. 2.— The Λ_{cl} Richness versus X-ray luminosity for the 31 PDCS cluster candidates in our sample. The squares are the detections and the arrows represent the 3σ upper limits. The solid line represents the fit to the L_x versus richness relation for Abell clusters taken from Briel & Henry (1993). The dashed line segments represent the median luminosity for Richness class 0, 1 & 2 Abell clusters presented in Burg *et al.* (1994). The lines have been adjusted to the passband of our survey and assume that Λ_{cl} is equivalent to the Abell richness. The top plot uses the richness values from the I_4 band while the bottom plot uses the richness values from the V_4 band.

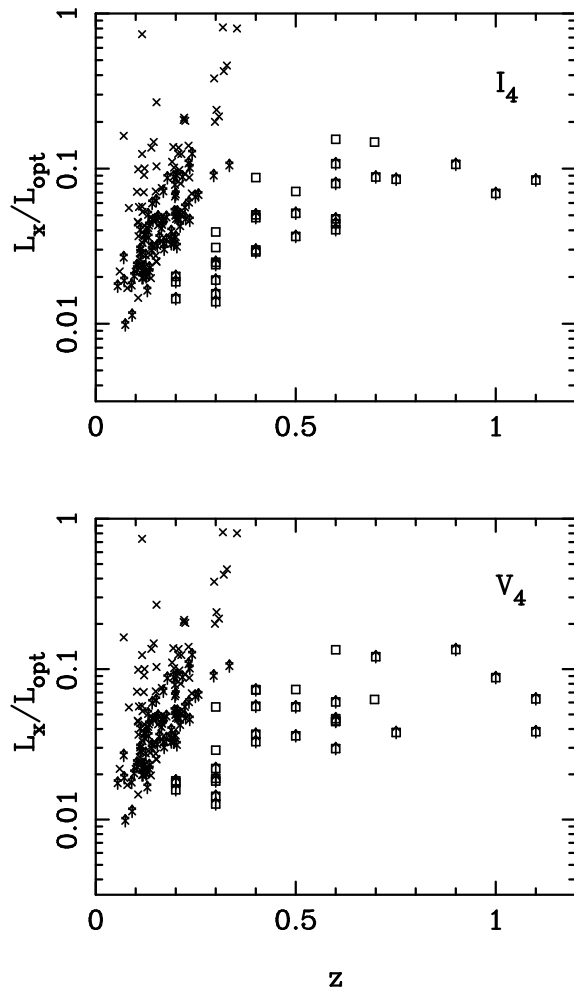


Fig. 3.— The optical luminosity to X-ray luminosity (L_{opt}/L_x) ratio versus redshift for the 31 PDCS cluster candidates in our survey and for the Abell clusters in the sample of Briel & Henry (1993). The squares are from our sample and the crosses are from the sample of Briel & and Henry 1993. Arrows through a symbol represent the 3σ upper limits from both samples. The top plot uses the richness values from the I_4 band while the bottom plot uses the richness values from the V_4 band.

